nature nanotechnology

SUPPLEMENTARY INFORMATION

https://doi.org/10.1038/s41565-019-0568-x

In the format provided by the authors and unedited.

A pH-responsive nanoparticle targets the neurokinin 1 receptor in endosomes to prevent chronic pain

Paulina D. Ramírez-García[1,2], Jeffri S. Retamal[1,2], Priyank Shenoy[1,2], Wendy Imlach[3], Matthew Sykes[3], Nghia Truong[1,2], Luis Constandil[4], Teresa Pelissier[4], Cameron J. Nowell[1], Song Y. Khor[1,2], Louis M. Layani[1,2], Chris Lumb[1,2], Daniel P. Poole[1,2], TinaMarie Lieu[1,2], Gregory D. Stewart[1], Quynh N. Mai[1,2], Dane D. Jensen[5], Rocco Latorre[5], Nicole N. Scheff[6], Brian L. Schmidt[6], John F. Quinn[1,2], Michael R. Whittaker[1,2], Nicholas A. Veldhuis[1,2]*, Thomas P. Davis[1,2,7]* and Nigel W. Bunnett[1,2,5,8]*

[1]Monash Institute of Pharmaceutical Sciences, Monash University, Parkville, Victoria, Australia. [2]Australian Research Council Centre of Excellence in Convergent Bio-Nano Science and Technology, Monash University, Parkville, Victoria, Australia. [3]Monash Biomedicine Discovery Institute, Monash University, Melbourne, Victoria, Australia. [4]Laboratory of Neurobiology, Center for the Development of Nanoscience and Nanotechnology (CEDENNA), University of Santiago de Chile, Santiago, Chile. [5]Departments of Surgery and Pharmacology, Columbia University Vagelos College of Physicians and Surgeons, Columbia University in the City of New York, New York , NY, USA. [6]Bluestone Centre for Clinical Research, New York University College of Dentistry, New York, NY, USA. [7]Australian Institute for Bioengineering and Nanotechnology, University of Queensland, Brisbane, Queensland, Australia. [8]Department of Pharmacology and Therapeutics, University of Melbourne, Parkville, Victoria, Australia. *e-mail: nicholas.veldhuis@monash.edu; thomas.p.davis@monash.edu; nwb2@nyu.edu

Supplementary Information

A pH-Responsive Nanoparticle Targets the Neurokinin 1 Receptor in Endosomes to Prevent Chronic Pain

Paulina D. Ramírez-García Jeffri S. Retamal, Priyank Shenoy, Wendy Imlach, Matthew Sykes, Nghia Truong, Luis Constandil, Teresa Pelissier, Cameron J. Nowell, Song Y. Khor, Louis M. Layani, Chris Lumb, Daniel P. Poole, TinaMarie Lieu, Gregory D. Stewart, Quynh N. Mai, Dane D. Jensen, Rocco Latorre, Nicole N. Scheff, Brian L. Schmidt, John F. Quinn, Michael R. Whittaker, Nicholas A. Veldhuis, Thomas P. Davis, Nigel W. Bunnett

Table of Contents

1. Supplementary Methods

1.1. Synthesis of diblock copolymers. Prior each synthesis, monomers were deinhibited using basic aluminium oxide. All polymers were synthesized via reversible addition fragmentation chain (RAFT) polymerization[1]. All reactions were carried out in toluene at 70°C and 400 RPM unless stated otherwise. Resulting polymers were purified by dialysis (molecular weight cut off, MWCO 3500, Membrane Filtration Products, USA) against acetone for 96 h. Residual solvent was evaporated and the final products were dried for 24 h in a vacuum oven at 37°C and 1000 mbar.

P(PEGMA-co-DMAEMA) hydrophilic block copolymer. The macromolecular chain transfer agent (macro-CTA), P(PEGMA-co-DMAEMA), was synthesized using 2-cyanoprop-2-yl dithiobenzoate (CPBD, 0.0736 g, $3.34 \cdot 10^{-4}$ mol) as a RAFT agent and azobisisobutyronitrile (AIBN, 0.0054 g, $3.34 \cdot 10^{-5}$ mol) as the initiator in a ratio of 1:0.1. The monomers poly(ethylene glycol) monomethyl ether methacrylate (PEGMA, 6 g, 0.02 mol) and 2-[*N,N*-(dimethylamino)ethyl] methacrylate (DMAEMA, 0.314 g, 0.001 mol) were added at a ratio of 10:1 and the mixture was left to react for 21 h.

P(PEGMA-co-DMAEMA)-b-P(DIPMA-co-DEGMA) diblock copolymer. The chain extension reaction was initiated by AIBN (0.0017 g, $1.033 \cdot 10^{-5}$ mol), using P(PEGMA-co-DMAEMA, 0.89 g, $6.89 \cdot 10^{-5}$ mol) and the monomers 2-[*N,N*-(diisopropylamino)ethyl] methacrylate (DIPMA, 1.47 g, $6.892 \cdot 10^{-3}$ mol) and di(ethylene glycol) methyl ether methacrylate (DEGMA, 0.1427 g, $7.58 \cdot 10^{-4}$) at a ratio of 0.15:1:100:11. The mixture was left to react for 17.5 h.

P(PEGMA-co-DMAEMA)-b-P(BMA) diblock copolymer. Butyl methacrylate (BMA, 0.582 g, 0.0041 mol) was polymerized from the hydrophilic P(PEGMA-co-DMAEMA) block by a chain extension reaction in the presence of AIBN (0.0008 g, $5.124 \cdot 10^{-6}$ mol) at a ratio of 120:1:0.2. The solution was left to react for 15 h.

P(PEGMA-co-DMAEMA)-b-P(DIPMA-co-DEGMA-co-Cy5) and P(PEGMA-co-DMAEMA)-b-P(BMA-co-Cy5) diblock copolymer. The chain extension of P(PEGMA-co-DMAEMA, 0.5 g, *$3.85 \cdot 10^{-5}$ mol*) was done by adding DIPMA (*0.82 g, $4.6 \cdot 10^{-3}$ mol)* and 4,4-dimethyl-2-vinyl-2-oxazolin-5-one (VDM, 0.027 g, *$1.92 \cdot 10^{-4}$ mol)* in the presence of AIBN (*0.95 mg, $5.77 \cdot 10^{-6}$ mol)* at a ratio of *1:100:11:5:0.15.* The mixture was left to react for *18 h.* For the BMA diblock copolymer only *BMA (0.66 g, 3.87·10-3 mol) was added* and the ratios of macro-CTA:BMA:VDM:AIBN were *1:120:5:0.15 and t*he mixture was left to react for *19* h. Cy5 coupling was achieved by mixing 250 µL of the reaction with Cyanine 5 amine (Cy5, 0.008 g, $1.20 \cdot 10^{-5}$ moles) and reacting at room temperature, 400 RPM for 72 h under dark conditions.

1.2. Analysis of diblock copolymers

Gel permeation chromatography. The molecular weights of polymers were determined by gel permeation chromatography using a Shimadzu (Kyoto, Japan) liquid chromatography system (Shimadzu, Japan) equipped with a (RID-10A) differential refractive index detector and SPD-20A ultraviolet-visible detector (λ = 633 nm). Samples were fractionated using 5.0 µm bead-size guard column (50 × 7.8 mm) and three Shodex KF-805L columns (300 × 8 mm, 10 µm bead-size, 5000 Å pore size) in series at 40°C. The eluent used was *N,N*-dimethylacetamide (DMAC, HPLC grade, with 0.03% w/v LiBr) with a flow rate of 1 mL/min. A molecular weight calibration curve was produced using polystyrene standards with narrow molecular weights distribution ranging from

500 to 2 × 10^6 Da.

Proton-nuclear magnetic resonance (^{1}H-NMR). The conversion of polymers was assessed by ^{1}H-NMR analysis using a Bruker Avance III 400 Ultrashield Plus spectrometer (USA) at 400 mHz running Topspin, version 1.3, using deuterated chloroform (chloroform-d) as solvent. Conversions (Conv%) and repeating monomer units (n) were calculated by ^{1}H-NMR using peak integrals (I) where the subscript number indicates the location of the peak in ppm (I_x). The Conv% and n for P(PEGMA-co-DMAEMA) were calculated using the ^{1}H-NMR spectra (Supplementary Fig. 1D.i) with $Conv\% = 100 \times \frac{(I_{4-4.6} - I_{5.7})}{I_{4-4.6}}$, $n_{PEGMA} = \frac{I_{4.25} - I_{2.5}}{I_{7.8-7.9}}$ and $n_{DMAEMA} = \frac{I_{2.5}}{I_{7.8-7.9}}$. Conv% and n for P(PEGMA-co-DMAEMA)-b-(DIPMA-co-DEGMA) were calculated using the ^{1}H-NMR spectra (Supplementary Fig. 1D.ii) with $Conv\% = 100 \times \frac{(PEGMA\,n + DEGMA\,n)}{(PEGMA\,n_{theoretical} + DEGMA\,n_{theoretical})}$, $n_{DIPMA} = \frac{I_3 + I_{2.6}}{2 \times I_{4-4.}} \times (n_{PEGMA} + n_{DMAEMA})$ and $n_{DEGMA} = \frac{I_{3.396}}{I_{3.378}} \times n_{PEGMA}$. Conv% and n for P(PEGMA-co-DMAEMA)-b-(BMA) were calculated using the ^{1}H-NMR spectra (Supplementary Fig. 1D.iii) with $Conv\% = 100 \times \frac{BMA\,n}{BMA\,n_{theoretical}}$ and $BMA\,n = \frac{I_{3.93}}{I_{4-4.2}} \times (PEGMA\,n + DEGMA\,n)$. Conv% and n for P(PEGMA-co-DMAEMA)-b-(DIPMA-co-DEGMA-co-VDM) and *P(PEGMA-co-DMAEMA)-b-(BMA-co-VDM)* were calculated as described for P(PEGMA-co-DMAEMA)-b-(DIPMA-co-DEGMA) *and P(PEGMA-co-DMAEMA)-b-(BMA)* (^{1}H-NMR spectra not shown).

1.3. Self-assembly of nanoparticles. P(PEGMA-co-DMAEMA)-b-P(DIPMA-co-DEGMA) was used as the diblock copolymer to self-assemble pH-responsive nanoparticles. P(PEGMA-co-DMAEMA)-b-P(BMA) was used to self-assemble control nanoparticles without pH responsive properties. For the self-assembly of nanoparticles loaded with aprepitant, a mixture of 5 mg of diblock copolymer and 53.5, 26.75 or 13.375 µg of aprepitant was dissolved in 0.5 mL of tetrahydrofuran (THF). Empty (Ø) nanoparticles were self-assembled without adding aprepitant. The mixture was then added into 4.5 mL of phosphate-buffered saline (PBS) under vigorous stirring at a flow rate of 1.2 mL/h, using a Harvard Apparatus syringe pump (USA) at room temperature. pH-responsive nanoparticles loaded with aprepitant (DIPMA-AP) and non-pH responsive nanoparticles loaded with aprepitant (BMA-AP) were dialyzed against PBS under nitrogen flow for 24 h (MWCO 3500). Assemblies without aprepitant (DIPMA-Ø and BMA-Ø) were dialyzed using Slide-A-Lyzer mini dialysis devices MWCO 3.5K (Thermo Fisher Scientific, USA) for 24 h. The assembly of nanoparticles for live cell imaging and biodistribution studies was done as described for nanoparticles without aprepitant using P(PEGMA-co-DMAEMA)-b-P(DIPMA-co-DEGMA-co-Cy5) *and P(PEGMA-co-DMAEMA)-b-(BMA-co-Cy5)*, which include Cy5 on the hydrophobic portion, resulting in nanoparticles with Cy5 localized in the core (DIPMA-Cy5 and BMA-Cy5).

1.4. Characterisation of nanoparticles

Dynamic light scattering (DLS). The size distribution of nanoparticles was determined by DLS using a Zetasizer Nano ZS ZEN3600 particle size analyser (Malvern, UK). DIPMA-AP, DIPMA-Ø and BMA-AP (1 mg/mL) were added to polystyrene cuvettes. Light scattering was measured at 25°C and 173° backscatter angle.

Ultra-performance liquid chromatography mass spectrometry (LC-MS). Aprepitant loading was assessed by LC-MS using a Waters Micromass Quattro Premier triple quadrupole mass spectrometer coupled to a Waters Acquity UPLC (USA). Freeze-dried DIPMA-AP and BMA-AP (1 mg/mL) were dissolved in a 5:2 mixture of DMSO:0.1% formic acid in water. Samples were prepared for analysis by mixing an aliquot with internal standard solution (diazepam, 5 µg/mL) in a 5:2 ratio and making up to 500 µL with the dilution solvent (1:1 mixture of 50% acetonitrile and 0.1% formic acid). Samples were fractionated on a Supelco Ascentis Express RP Amide column

(50 mm by 2.1 mm, 2.7 µm particle size) equipped with a Phenomenex SecurityGuard precolumn fitted with a Synergi Polar cartridge. Aprepitant loading was quantified against aprepitant standards (0.016 to 20 µM). The mobile phase consisted of 0.05% formic acid in water and acetonitrile and compounds were eluted under gradient conditions. Mass spectrometry was conducted in positive electrospray ionization conditions and elution of compounds monitored with multiple-reaction monitoring.

Determination of critical micelle concentration. The critical micellar concentration was determined by the pyrene I_1/I_3 ratio[2]. A pyrene stock solution (50 µM) was prepared in THF and 5 µL of pyrene stock were added to 995 µL of graded concentrations of nanoparticles (400 to 0.5 µg/mL), obtained by diluting nanoparticle stock solutions in PBS. The mixture was stirred for 3 h at room temperature and the fluorescence spectrum of pyrene was recorded from 360 to 410 nm using an excitation wavelength of 336 nm in a RF5301PC Espectrofluorophotometer (Shimadzu, Japan). The emission intensities measured at 373 nm (I_1) and 384 nm (I_3) were used to calculate the pyrene I_1/I_3 ratio.

Transmission electron microscopy. The morphology of nanoparticles was determined by transmission electron microscopy imaging using a Tecnai F20 transmission electron microscope at an accelerating voltage of 200 kV at ambient temperature. An aliquot (5 µL) of 0.1 wt% nanoparticle solution (diluted with Milli-Q water) was deposited on a Formvar coated copper grid (GSCu100F-50, Proscitech, Australia) and was allowed to dry overnight in air and at room temperature.

1.5. Nanoparticle disassembly. Nile Red (NR) is a solvatochromic dye that fluoresces only in non-polar solvents, allowing determination of the pH of disassembly for the nanoparticles. Specifically, the pH of disassembly is identified by observing the loss of fluorescence of NR due to release of NR from the core of nanoparticles. Nanoparticles were self-assembled using 0.1 mg of NR per mg of polymer and dialyzed as previously described. pH-responsive nanoparticles loaded with Nile red (DIPMA-NR) and non-pH responsive nanoparticles loaded with NR (BMA-NR) were prepared at a concentration of 200 µg/mL. For pH-dependent disassembly studies, nanoparticles were suspended in a mixture of 0.1 M citric acid and 0.2 M Na_2HPO_4 buffer solutions with a pH range from 7.6 to 5.0. pH-dependent disassembly was assessed by measuring NR fluorescence (excitation/emission 552/636nm) using a FlexStation 3 (Molecular Devices, USA). The time course of nanoparticle disassembly was examined by measuring NR fluorescence at pH 7.4, 6.5, 6.0 and 5.0 over a 12 h period using a CLARIOstar (BMG LABTECH, Germany).

1.6. pERK localization in mouse spinal cord. Spinal cord sections were preincubated in 10% normal donkey serum (NDS) in 0.1 M PBS (1 h, room temperature), followed by rabbit anti-phospho-p44/42 MAPK (ERK1/2) (Thr202/Tyr204) (1:200; #4370; Cell Signalling Technology, Danvers, MA) and guinea-pig anti-NeuN (1:1000, Millipore, #abN90) in PBS containing 0.3% Triton X-100 and 5% NDS (overnight, 4˚C). Sections were washed 4x in 0.1 M PBS containing 0.3% Triton X-100 and incubated with donkey anti-rabbit Alexa 488 and donkey anti-guinea-pig Alexa 568 (1:1000, Thermo Fisher Scientific) (45 min, room temperature). Sections were washed 5x in PBS, counter-stained with DAPI (10 µg/ml, 5 min) and cover-slipped with ProLong Glass mounting medium (Thermo Fisher Scientific). Sections were imaged on Leica SP8 confocal microscope with HC PLAPO 40X for counting pERK-immunoreactive (IR) neurons or a 20X objective to collect representative images. For each experimental group, 6 sections of ipsilateral and contralateral dorsal horn were imaged. Only pERK-positive neurons co-labelled with NeuN were counted. To avoid re-counting the same neurons, the analysed sections were 100 µm apart. The total number of neurons was averaged for each group.

1.7. Rotarod test. A rotarod test was used to assess whether the intrathecal injection of nanoparticles would affect normal motor function and thereby impede studies of nociception that

require examination of paw withdrawal from a painful stimulus. Prior to experiments, mice were acclimatized and trained on the rotarod apparatus for three consecutive runs on two successive days. On the day of the experiment, three baseline readings were recorded and a cut-off threshold of 120 second was pre-set. Nanoparticles (DIPMA-AP, BMA-AP, DIPMA-Ø, 10 µg/mL) or vehicle (aCSF) was injected intrathecally as described above. Subsequently, the latency of mice to fall (seconds) were recorded at 30, 60, 90, 120, 180 and 240 min post-injection[3].

1.8. Electrophysiological assessment of nociception in rats. Rats were maintained under anaesthesia (1.2-1.5% isoflurane in oxygen using a diaphragm rodent facemask) and placed on a regulated thermal pad (37 ± 0.5°C). EMG activity was measured using a pair of platinum stimulation electrodes inserted subcutaneously into the lateral part of the third and fourth toes, and recording electrodes inserted through the skin into the ipsilateral biceps femoris muscle[4]. The C-reflex corresponds to the integration of the reflex response into a 150-450 ms time window post-stimulus. Wind-up is a potentiation of the C-reflex response when the stimulating frequency is increased to 1 Hz. The wind-up score corresponds to the slope of the first seven consecutive C-reflex recordings obtained at 1 Hz stimulation. After recording to obtain a stable C-reflex response (~30 min), the threshold for C-reflex was estimated and the rats remained stimulated at 2X the threshold intensity for the duration of the experiment. The C-reflex was evaluated by the mean of 15 consecutive stimuli at 0.1 Hz while the next 7 stimuli at 1 Hz were used to evaluate wind-up. Recordings were made 10 days after surgery before (basal) and 30, 60, 90 and 120 min after intrathecal drug administration. The integrated C-reflex responses were expressed as a percentage of basal response.

1.9. NK_1R localization in rat spinal cord. Free floating sections were blocked in PBS containing 0.3% Triton x-100 and 10% NDS (1 h, room temperature). Sections were incubated with rabbit anti-NK_1R (1:1000, #94168) and guinea-pig anti-NeuN (1:1000, Millipore, abn90) in PBS containing 0.3% Triton X-100 and 3% NDS (overnight, 4°C). Sections were washed 4x in PBS and incubated with donkey anti-rabbit Alexa488 and donkey anti-guinea-pig Alexa568 (1:1000, Thermo Fisher Scientific) (2 h, room temperature). Sections were washed 5x in PBS, counter stained with DAPI (10 µg/ml, 5 min), and mounted onto ColorFrost Plus slides (VWR) with ProLong Glass mounting medium (Thermo Fisher Scientific). Sections were imaged on Leica SP8 confocal microscope with a HC PL APO 63x oil objective (NA 1.4). Z stacks of NK_1R-positive neurons in lamina I of the dorsal horn were collected with a digital zoom of 5. To quantify NK_1R endocytosis in lamina I neurons, the border of the cytoplasm of the soma was delineated by NeuN fluorescence. NK_1R immunoreactivity within 5 pixels (0.5 µm) of the border was defined as plasma membrane receptor. The ratio of plasma membrane to cytosolic NK_1R-IR fluorescence was determined in >6 lamina I neurons per condition.

1.10. Cell viability assays. HEK-hNK_1R cells were incubated with empty nanoparticles (1-100 µg/mL) for 24 and 48 h. Medium was replaced by phenol red-free DMEM, followed by incubation for 2 h (37°C, 5% CO_2) with 10% (v/v) alamarBlue reagent (Thermo Fisher Scientific, USA). Fluorescence of the reduced active compound, resofurin, was measured (510/610nm exc/em) using a ClarioStar (BMG LABTECH, Germany).

Supplementary Figures

A

Polymer	Conversion (%)	GPC Mn (g/mol)	GPC PDI	^{1}H-NMR Mn (g/mol)	^{1}H-NMR Composition PEGMA	DMAEMA	DIPMA	DEGMA	BMA
P(PEGMA-co-DMAEMA)	54	12,377	1.20	17,600	56	6	-	-	-
P(PEGMA-co-DMAEMA)-b-(DIPMA-co-DEGMA)	92	17,581	1.36	39,444	56	6	91	12	-
P(PEGMA-co-DMAEMA)-b-P-(BMA)	82	18,225	1.37	31,654	56	6	-	-	98
P(PEGMA-co-DMAEMA)-b-(DIPMA-co-DEGMA-co-VDM)	95	19,380	1.22	39,881	56	6	95	11	-
P(PEGMA-co-DMAEMA)-b-P-(BMA-co-VDM)	62	18,576	1.29	28,220	56	6	-	-	74

B Raft polymerization of diblock copolymers

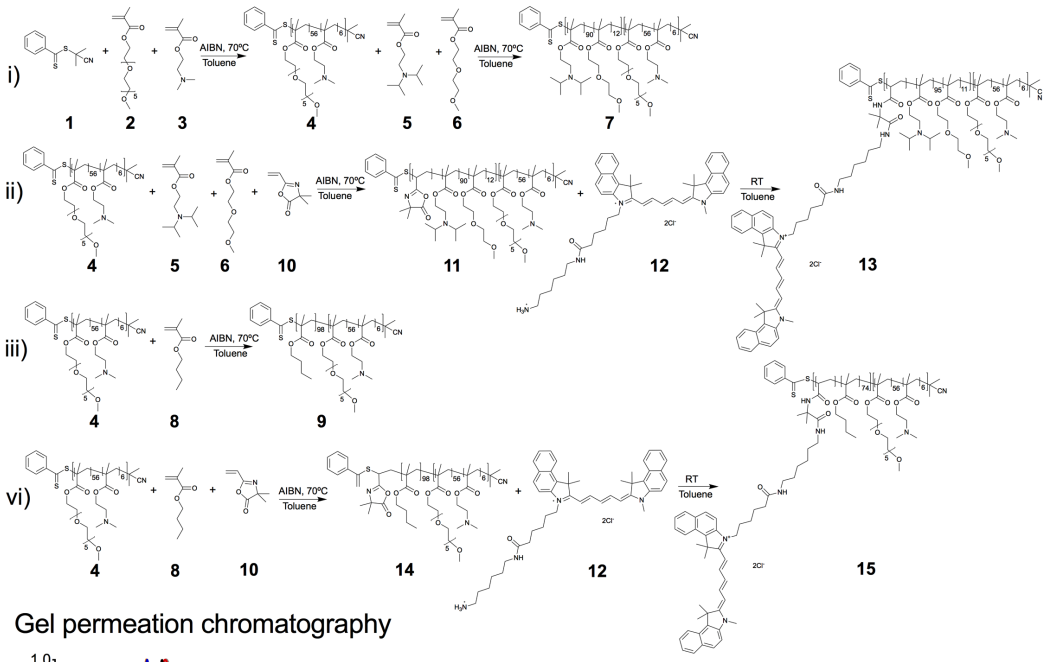

C Gel permeation chromatography

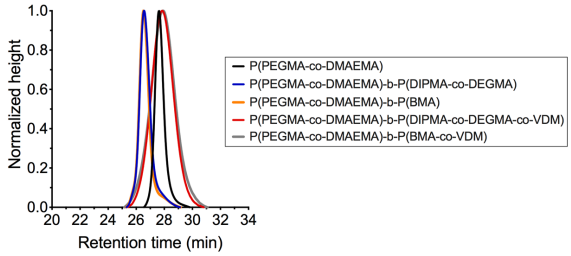

D Proton nuclear magnetic resonance

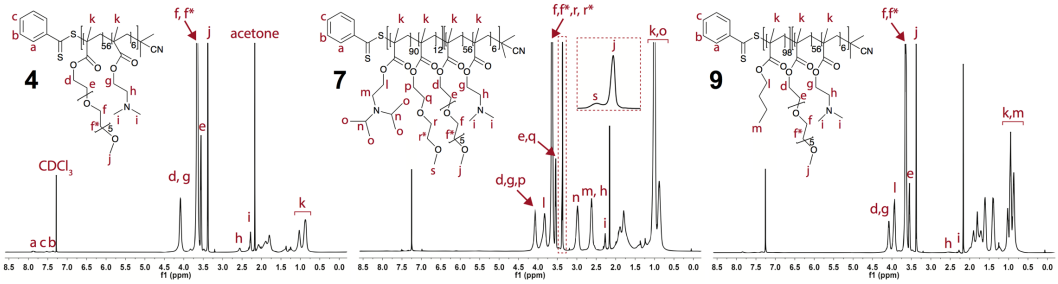

Figure S1. Synthesis and characterization of P(PEGMA-co-DMAEMA)-b-P(DIPMA-co-

DEGMA) and P(PEGMA-co-DMAEMA)-b-P(BMA-co-DEGMA) diblock copolymers. A. Characterization of the hydrophilic block copolymers and the diblock copolymers. **B. i)** Sequential RAFT polymerization indicating synthesis of the hydrophilic block using (**1**) CPDB, (**2**) PEGMA and (**3**) DMAEMA to form (**4**) p(PEGMA-c-DMAEMA); synthesis of P(PEGMA-co-DMAEMA)-b-P(DIPMA-co-DEGMA) by chain extension reaction, where addition of the pH-responsive monomer (**5**) DIPMA and the charge screening monomer (**6**) DEGMA to (**4**) the hydrophilic block forms (**7**) the diblock P(PEGMA-co-DMAEMA)-b-P(DIPMA-co-DEGMA); **ii)** Addition of (**5**) DIPMA, (**6**) DEGMA and (**10**) VDM to (**4**) the hydrophilic block to form the intermediate (**11**), followed by the addition of (**12**) Cy5 to form the final Cy5 conjugated polymer (**13**) P(PEGMA-co-DMAEMA)-b-P(DIPMA-co-DEGMA-co-Cy5). **iii)** Addition of (**8**) BMA to (**4**) the hydrophilic block forms (**9**) P(PEGMA-co-DMAEMA)-b-P(BMA). **iv)** Addition of (**8**) BMA and (**10**) VDM to (**4**) the hydrophilic block to form the intermediate (**14**), followed by the addition of (**12**) Cy5 to form the final Cy5 conjugated polymer (**15**) P(PEGMA-co-DMAEMA)-b-P(BMA-co-Cy5). **C.** Gel permeation chromatography traces showing a shift from P(PEGMA-co-DMAEMA) to higher molecular weight (*i.e.*, shorter retention time) after chain extension to form P(PEGMA-co-DMAEMA)-b-P(DIPMA-co-DEGMA) and P(PEGMA-co-DMAEMA)-b-P(BMA-co-DEGMA). **D.** ^{1}H-NMR spectra of the resulting polymers indicating the successful incorporation of the monomers. ^{1}H-NMR was used to estimate molecular weight since gel permeation chromatography was calibrated using polystyrene standards. **C** and **D** are from a single independent experiment because the polymer was made once and used throughout the project.

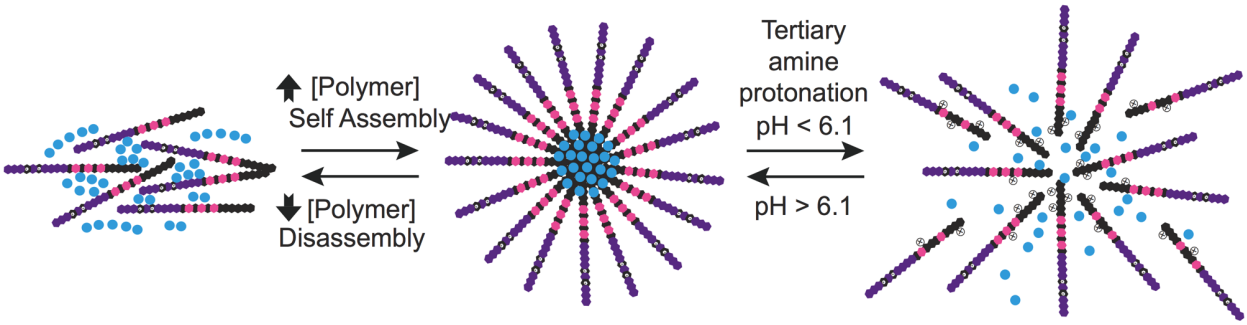

Figure S2. Mechanism of concentration-dependent self-assembly and pH-dependent disassembly of DIPMA nanoparticles. Increasing concentrations of polymer result in nanoparticle self-assembly in an aqueous solution. DIPMA nanoparticles possess a tertiary amine on the DIPMA units located in the core. At pH<6.1, protonation results in a change from neutral to positive charge on DIPMA that induce like-like charge repulsion, which destabilizes the nanoparticle core with the subsequent disassembly and release of cargo.

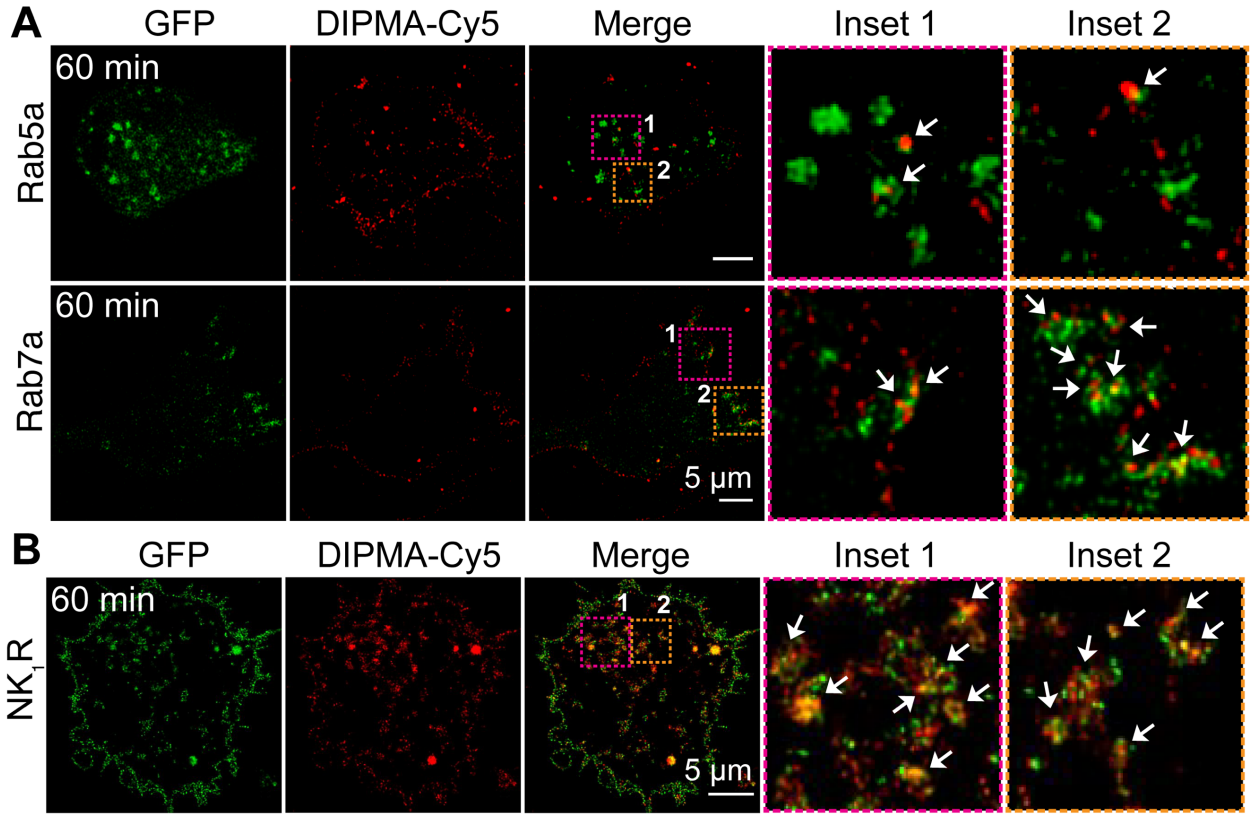

Figure S3. Uptake of DIPMA-Cy5 nanoparticles in HEK-293 cells. A. Localization of DIPMA-Cy5 nanoparticles in Rab5a-GFP early endosomes and Rab7a-GFP late endosomes after incubation with HEK-293 cells for 60 min. Representative results, *n* = 5 independent experiments. **B.** Colocalization of DIPMA-Cy5 nanoparticles and NK_1R-GFP in HEK-rNK_1R cells at 60 min after stimulation with SP to induce NK_1R endocytosis. Representative results, *n* = 5 independent experiments.

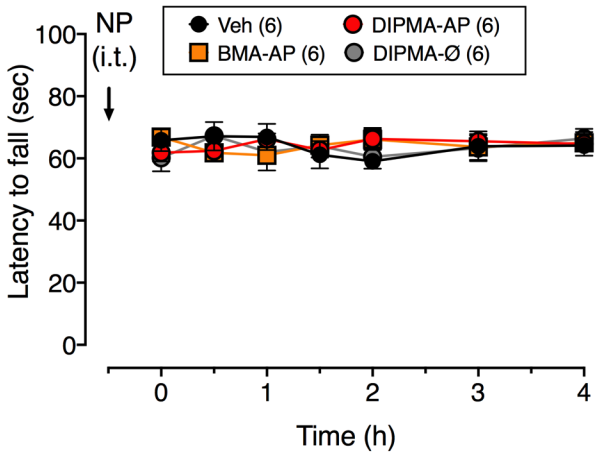

Figure S4. Effects of nanoparticles on rotarod latency. Effects of intrathecal (i.t.) injection of vehicle (Veh), DIPMA-Ø, BMA-AP or DIPMA-AP nanoparticles (NP) on latency to fall in mice, assessed using rotarod. Data are presented as mean ± SEM from *n* = 6 mice (numbers in parentheses) for each treatment group.

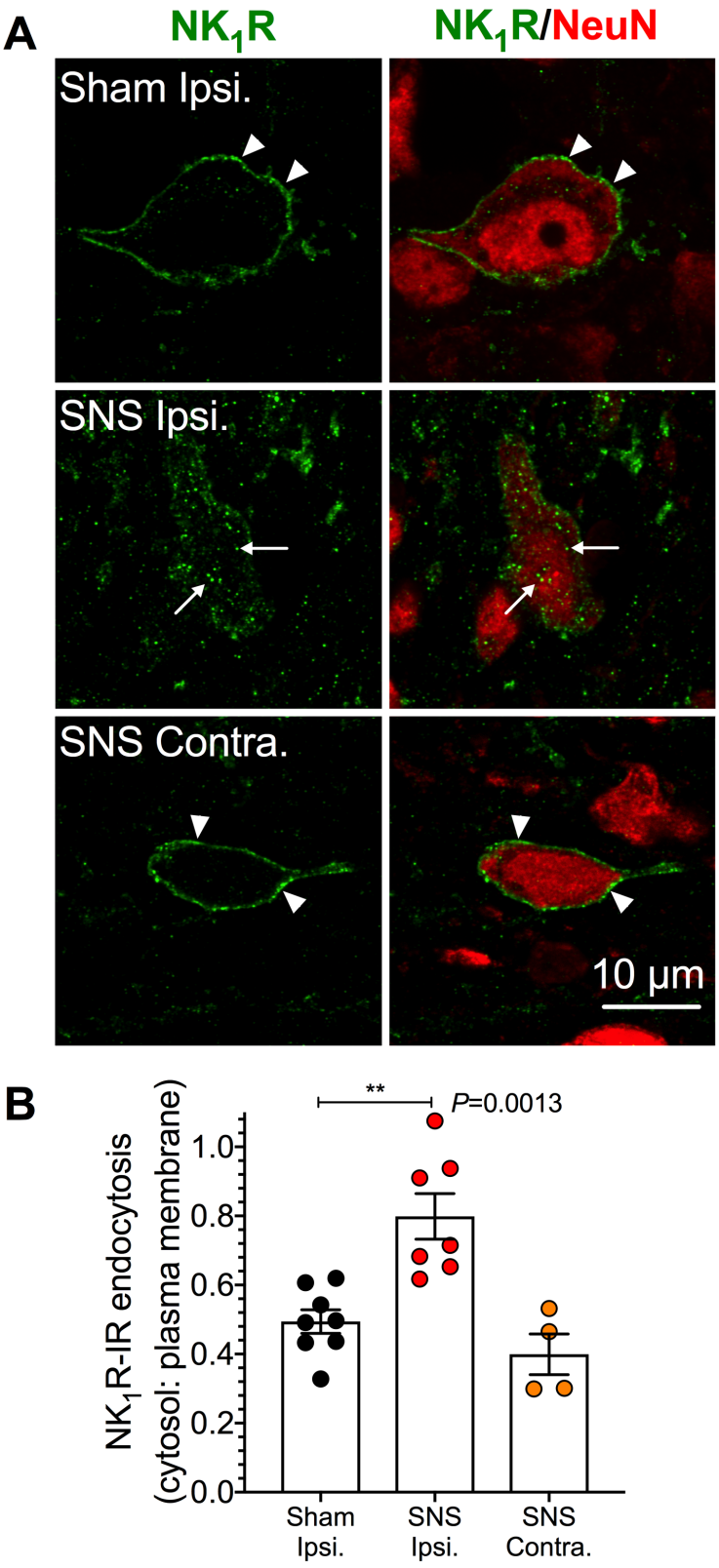

Figure S5. NK_1R endocytosis in chronic neuropathic nociception. To confirm activation of the SP/NK_1R system during chronic neuropathic nociception, the NK_1R was localized in the dorsal

horn of rats 10 days after sural nerve spared (SNS) or sham surgery by immunofluorescence. **A.** Localization of NK_1R-IR and NeuN-IR to the ipsilateral (Ipsi.) or contralateral (Contra.) lamina I dorsal horn of sham or SNS rats. Arrow heads denote plasma membrane. Arrows denote endosomes. **B.** Quantification of NK_1R endocytosis, assessed as the cytosol:plasma membrane pixel intensity for NK_1R-IR neurons. Data are presented as mean ± SEM from sham ipsilateral (*n* = 8 rats), SNS ipsilateral (*n* = 7 rats) and SNS contralateral (*n* = 4 rats) groups. 1-way ANOVA, non-parametric Tukey post-hoc test. $^{**}P<0.01$.

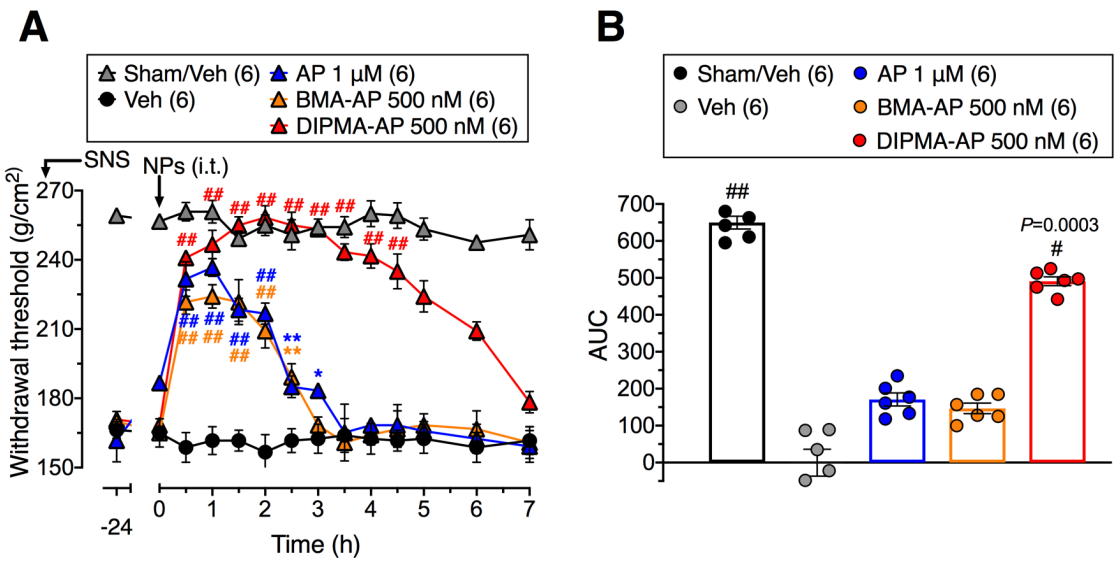

Figure S6. Effects of nanoparticles on neuropathic nociception. The sural nerve spared (SNS) model of chronic neuropathic pain was studied in rats. Vehicle (Veh), aprepitant (AP) or nanoparticle (NP) was administered by intrathecal injection 10 days after SNS or sham surgery. Paw withdrawal responses were assessed using the Randall-Selitto test. **A.** Time course of response. **B.** Area under curve (AUC) from 0-7 h. Data are presented as mean ± SEM from n = 6 rats (numbers in parentheses) for each treatment group. *P<0.05, **P<0.005, $^{\#}P$<0.001, $^{\#\#}P$<0.0001 compared to SNS vehicle. 1-way ANOVA, nonparametric Dunn's post-hoc test.

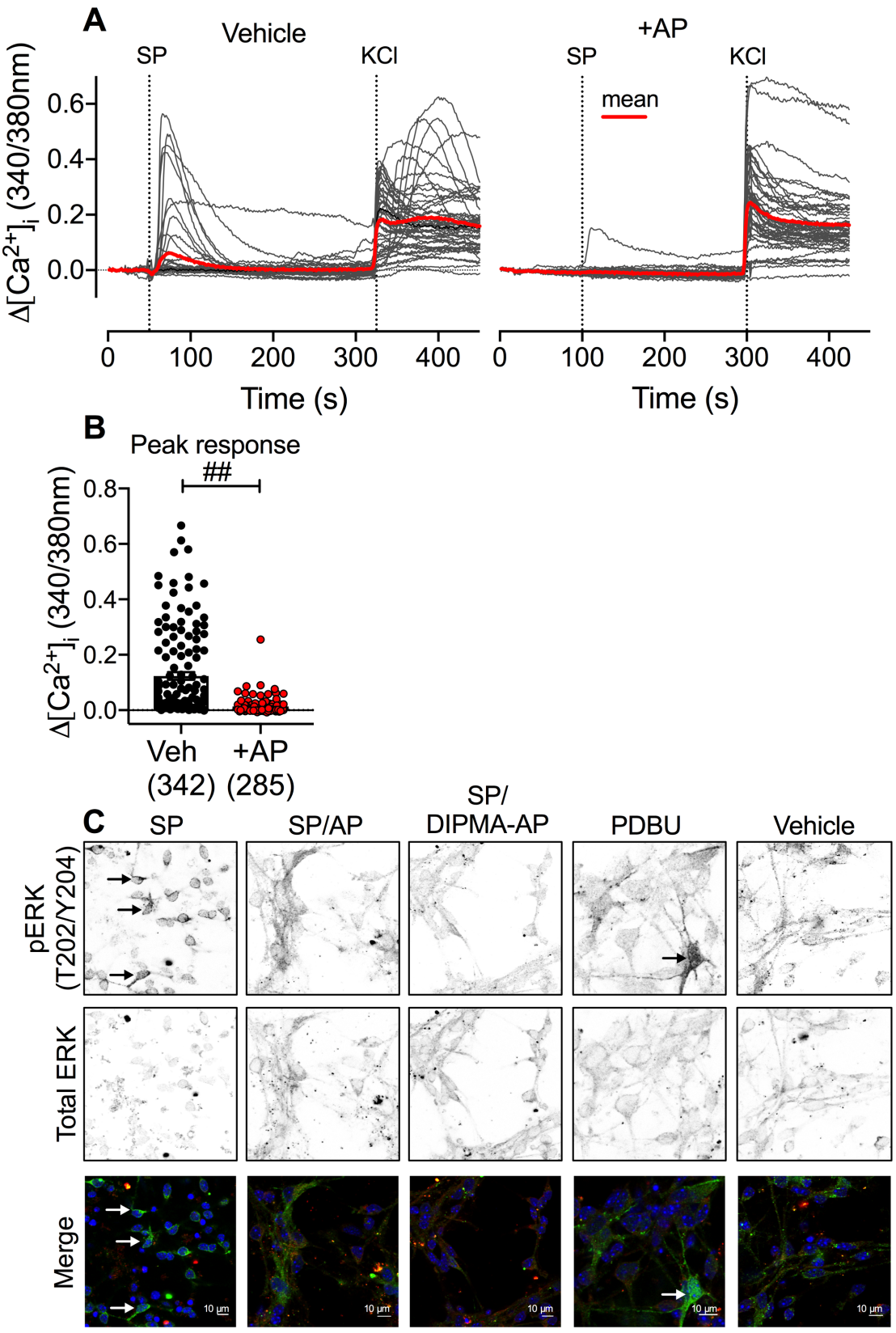

Fig. S7. SP signaling in mouse striatal neurons. SP (100 nM)-induced Ca^{2+} signaling in striatal

neurons pretreated with vehicle (Veh) or aprepitant (AP). **A.** Representative traces of $[Ca^{2}+]_{i}$. Grey lines show responses of individual neurons. Red lines show mean responses. **B.** Peak $[Ca^{2}+]_{i}$ responses. Data are expressed as mean ± SEM from *n* = 342 neurons for SP plus vehicle or *n* = 285 neurons for SP plus aprepitant (numbers in parentheses) from *n* = 3 independent experiments for both treatment groups. ##*P*<0.0001, unpaired *t*-test (2-tailed). **C.** Representative images of phospho-ERK and total ERK immunostaining in cultured striatal neurons from *n* = 3 independent experiments. Neurons were treated with SP, SP plus aprepitant (AP), SP plus DIPMA-AP, phorbol 12,13-dibutyrate (PDBU) or vehicle.

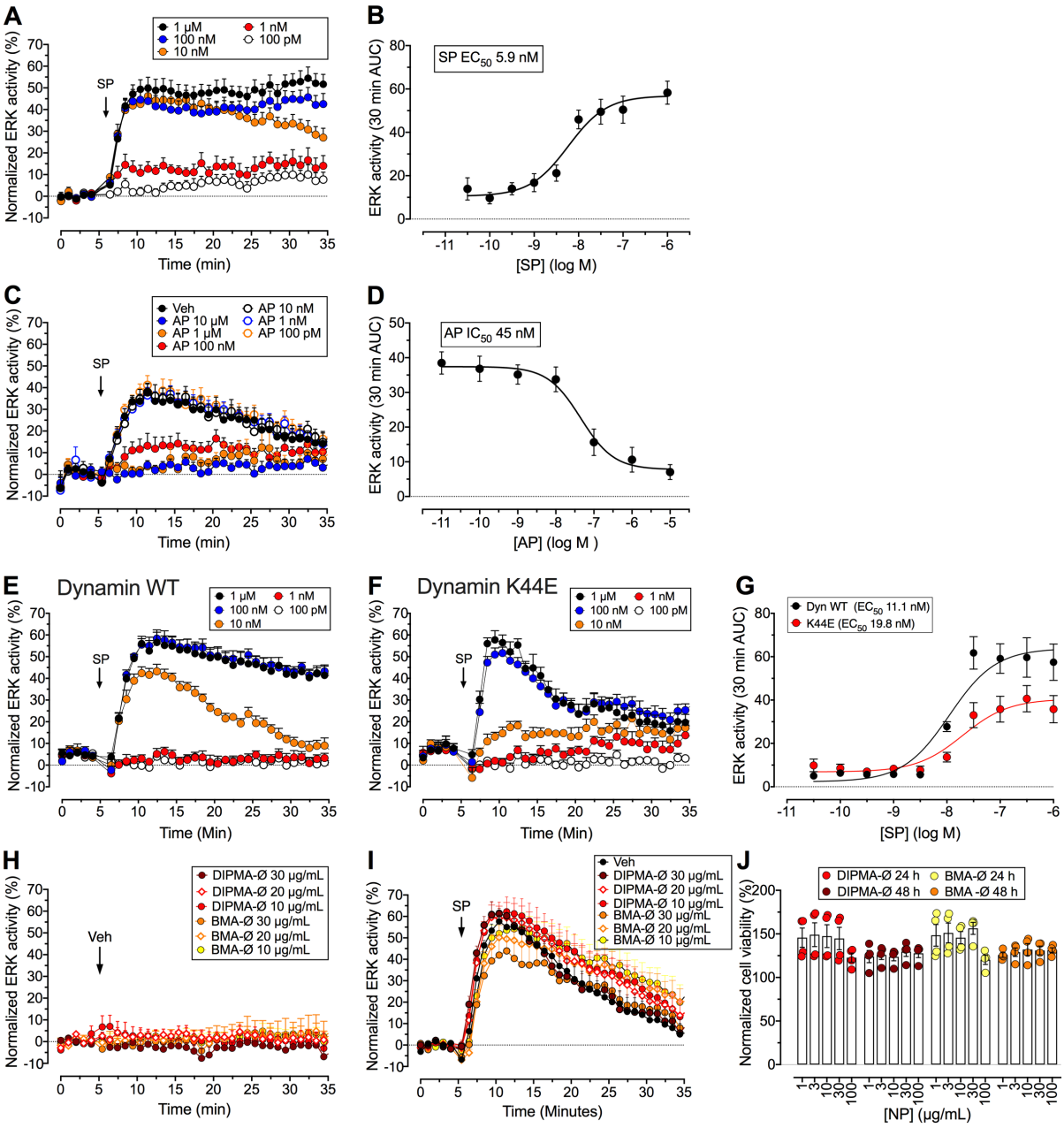

Figure S8. Nuclear ERK signalling and toxicity assays in HEK-293 cells. A-I. SP activation of nuclear ERK in HEK-hNK$_1$R cells. To examine activation of nuclear ERK, HEK-293 cells expressing hNK$_1$R were transfected with NucEKAR (FRET biosensor for nuclear ERK). Data are expressed as mean ± SEM, with triplicate observations made in each experiment. **A.** Effects of graded concentrations of SP on nuclear ERK activity; *n* = 8 independent experiments. **B.** SP concentration-response curves; *n* = 8 independent experiments. **C.** Effects of graded concentrations of aprepitant (AP) on nuclear ERK response to SP (5 nM); *n* = 7 independent experiments. **D.** Aprepitant concentration-response curves; *n* = 7 independent experiments. **E-G.** SP-induced activation of nuclear ERK in HEK-hNK$_1$R cells expressing dynamin wildtype (Dyn WT, **E**) or dynamin K44E (Dyn K44E, **F**); *n* = 6 independent experiments. **G.** SP concentration-response curves; *n* = 6 independent experiments. **H, I.** Effects of DIPMA-Ø and BMA-Ø on basal nuclear ERK activity in HEK-293 cells (**H**) and on SP-stimulated nuclear ERK activity in HEK-

hNK$_1$R cells (**I**) over 30 min; *n* = 7 independent experiments. **J.** Effects DIPMA-Ø and BMA-Ø on viability of HEK-293 cells over 24 h and 48 h. Viability was examined using alamarBlue, which assess the capability of viable cells to reduce rezasurin to resofurin; triplicate observations, *n* = 4 independent experiments.

Supplementary Videos

Video S1. Localization of DIPMA-Cy5 nanoparticles and Rab5a-GFP in HEK-293 cells. The video shows trafficking of DIPMA-Cy5 nanoparticles (red) to Rab5a-GFP early endosomes (green). Cells were incubated with DIPMA-Cy5 nanoparticles for 30 min.

Video S2. Localization of DIPMA-Cy5 nanoparticles and Rab7a-GFP in HEK-293 cells. The video shows trafficking of DIPMA-Cy5 nanoparticles (red) to Rab7a-GFP late endosomes (green). Cells were incubated with DIPMA-Cy5 nanoparticles for 30 min.

Video S3. Localization of DIPMA-Cy5 nanoparticles and NK_1R-GFP in HEK-293 cells. The video shows trafficking of DIPMA-Cy5 nanoparticles (red) and NK_1R-GFP (green). Cells were incubated with DIPMA-Cy5 nanoparticles for 90 min and with SP for 60 min to induce NK_1R endocytosis.

Video S4. Localization of DIPMA-Cy5 nanoparticles in the mouse dorsal horn. The video is a 3D projection of DIPMA-Cy5 nanoparticles in the perinuclear region of lamina I cells in the dorsal horn of the mouse spinal cord. The image was taken at 1 h after intrathecal injection of nanoparticles. Nuclei are stained with DAPI.

Video S5. Localization of BMA-Cy5 nanoparticles in the mouse dorsal horn. The video is a 3D projection of BMA-Cy5 nanoparticles in the perinuclear region of lamina I cells in the dorsal horn of the mouse spinal cord. The image was taken at 1 h after intrathecal injection of nanoparticles. Nuclei are stained with DAPI.

Video S6. Localization of NK_1R-IR in the rat dorsal horn after sham surgery. The video is a 3D projection showing the subcellular localization of NK_1R-IR (green) of lamina I spinal neuron (NeuN, red). The image was taken at 10 days after sham surgery.

Video S7. Localization of NK_1R-IR in the rat dorsal horn after SNS surgery. The video is a 3D projection showing the subcellular localization of NK_1R-IR (green) of lamina I spinal neuron (NeuN, red). The images were taken at 10 days after SNS surgery.

Supplementary References

1. Chiefari, J.*, et al.* Living free-radical polymerization by reversible addition−fragmentation chain transfer: The raft process. *Macromolecules* **31,** 5559-5562 (1998)

2. Aguiar, J., Carpena, P., Molina-Bolívar, J. A. & Carnero Ruiz, C. On the determination of the critical micelle concentration by the pyrene 1:3 ratio method. *J. Coll. Inter. Sci.* **258,** 116-122 (2003)

3. Jensen, D. D.*, et al.* Neurokinin 1 receptor signaling in endosomes mediates sustained nociception and is a viable therapeutic target for prolonged pain relief. *Sci. Trans. Med.* **9,** eaal3447 (2017)

4. Bravo, D.*, et al.* Pannexin 1: A novel participant in neuropathic pain signaling in the rat spinal cord. *Pain* **155,** 2108-2115 (2014)